DOI:10.1190/segam2017-17690973.1

Wave-equation tomography with surface offset gathers by plane-wave encoding

Yujin Liu, Yan Wu*, Xiongwen Wang*, Tong W. Fei† and Yi Luo†*
**Aramco Research Center−Beijing, Aramco Asia, Beijing, China*
†*EXPEC Advanced Research Center, Saudi Aramco, Dhahran, Saudi Arabia*

SUMMARY

Common image gather (CIG) extraction is an important procedure for velocity analysis. Surface offset gathers (SOGs) provide longer and more reliable sampling of residual curvature than other CIGs, such as angle gathers, particularly those from deep events, which is useful for building the deep part of the velocity model. SOGs are available after application of Kirchhoff depth migration to properly sorted seismic data cubes with little extra cost, while it's very costly to compute from wave-equation (WE) migration directly. In this abstract, we apply plane-wave encoding to improve the efficiency of SOG extraction from WE migration. Geometric analysis demonstrates the equivalence of plane-wave SOGs and standard SOGs. Numerical tests show that our proposed method can efficiently extract SOGs with reliable residual moveout (RMO) information. We also use plane-wave SOGs in WE tomography and compare it with WE tomography based on plane-wave domain CIGs. Preliminary inversion results show its potential in improving subsalt velocity building.

INTRODUCTION

Common image gathers (CIGs) play an important role in migration velocity analysis. There are two major types of CIGs used in the industrial ray tomography, including surface offset gathers (SOGs) and angle domain common image gathers (ADCIGs). ADCIGs are less prone to geometric artifacts and tackle complex propagation effects better, especially when multi-pathing occurs (Xu et al., 2001; Stolk and Symes, 2004). However, the maximum incident angle gradually decreases with depth to small values for the deepest reflectors, which will degrade the accuracy of velocity estimation. On the other hand, SOGs always contain the entire offset range and provide more reliable residual moveout (RMO) information. Recent work shows SOGs have better performance in subsalt tomography (Yang et al., 2015).

SOGs are available directly from common offset Kirchhoff depth migration without extra cost, while they are not straightforward to compute via WE migration. The conventional way is to divide the recorded data into offset groups and migration each group separately. This method is accurate but computationally very expensive. To improve the efficiency, Etgen (2012) proposed using 3D wave-equation Kirchhoff migration to extract SOGs. The method computes and saves the Green's functions from different surface positions, then it computes the migration operator and applies the operator to sorted data to form SOGs using saved Green's functions. The computational cost is also very high and I/O is a big burden. Giboli et al. (2012) adopted the idea of attribute migration to recover the surface offset information after dividing the image of the offset-scaled data by the image of the original data. Then SOGs can be extracted from the common shot migration image using the offset maps. The method needs only one extra migration in the 2D case and two extra migrations in the 3D case, which is much more efficient than earlier methods. However, it can't provide correct surface offset information when the velocity is wrong. Montel (2014) analyzed the kinematic behavior of SOGs using attribute migration and found it's different from standard offset domain migration.

Previous work mainly concentrated on SOG extraction from WE migration and used the RMO information with conventional ray tomography, but not WE tomography. There are some exceptions. Fleury et al. (2014) used SOGs from attribute migration to WE tomography. Zhang et al. (2014) used the conventional offset group method in WE tomography. However, all of them have either inaccuracy or inefficiency problems. In this work, we applied plane-wave encoding to decrease the computational cost without loss of accuracy. Stork et al. (2002) mentioned to use plane wave encoding to generate SOGs, but they didn't use it in WE tomography. Moreover, we found that it's possible to improve the efficiency further by optimal selection of plane-wave values for different offsets. The abstract is organized as follows: first, we review conventional SOG extraction and introduce the plane-wave encoding strategy. Then, we provide geometric analysis of plane-wave SOGs. After the extraction part, we derive the formulas for WE tomography using SOGs. At last, we show some numerical tests to demonstrate the effectiveness of the method.

THEORY

In this section, we will give the formulas of SOG extraction from WE migration by offset groups and plane wave encoding, analyse the geometric property of plane-waves in SOGs, and derive SOG-based WE tomography operator.

Surface offset gather extraction

WE migration generates a subsurface image by cross-correlating the source wavefield and receiver wavefield. The imaging condition can be expressed in the frequency domain as follows,

$$I(\mathbf{x},\mathbf{x}_s) = \int S(\mathbf{x},\omega;\mathbf{x}_s)R^*(\mathbf{x},\omega;\mathbf{x}_s)d\omega \qquad (1)$$

where $S(\mathbf{x},\omega;\mathbf{x}_s)$ is the forward propagated wavefield from source $\mathbf{x}_s$. Then, for a given shot $\mathbf{x}_s$, back-propagating all receiver traces at the same time yields the wavefield $R^*(\mathbf{x},\omega;\mathbf{x}_s)$, where $*$ denotes the complex-conjugate. In this way, the cost is reduced, but offset information is lost. By introducing the single-trace wavefield $R^*(\mathbf{x},\omega;\mathbf{x}_r,\mathbf{x}_s)$ from source at $\mathbf{x}_s$ and

receiver at $\mathbf{x}_r$, we can rewrite equation 1 as,

$$I(\mathbf{x},\mathbf{x}_s) = \int S(\mathbf{x},\omega;\mathbf{x}_s) \int R^*(\mathbf{x},\omega;\mathbf{x}_r,\mathbf{x}_s) d\mathbf{x}_r d\omega \qquad (2)$$

A trivial way to compute surface offset gathers would be to migrate each trace separately, and then to sort the images according to the offset $\mathbf{h} = (\mathbf{x}_r - \mathbf{x}_s)/2$. That is,

$$I(\mathbf{x},\mathbf{h}) = \int\int S(\mathbf{x},\omega;\mathbf{x}_s) R^*(\mathbf{x},\omega;\mathbf{h},\mathbf{x}_s) d\mathbf{x}_s d\omega \qquad (3)$$

If we only consider the cost of reconstructing wavefields by solving the wave-equation, the computational cost of equation 3 is about $ns + nh * ns$ times solving for the wave propagation, which is a prohibitive task.

To improve the efficiency, we apply plane-wave encoding defined as,

$$I(\mathbf{x},\mathbf{h}) = \int\int S(\mathbf{x},\omega;\mathbf{p}_s) R^*(\mathbf{x},\omega;\mathbf{h},\mathbf{p}_s) d\mathbf{p}_s d\omega \qquad (4)$$

The computational cost is about $np + nh * np$ wave propagation solutions.

Moreover, if we analyze the kinematic behaviour of plane-wave propagation for a specific offset, we can find that only some portions of plane-waves contribute to the final SOG. Figure 1 shows that only two plane-waves are needed in the simple case of two flat layers. We also find that even in the case of a complex subsurface model, half the plane-waves needed in the conventional plane-wave migration (Zhang et al., 2005) are often sufficient.

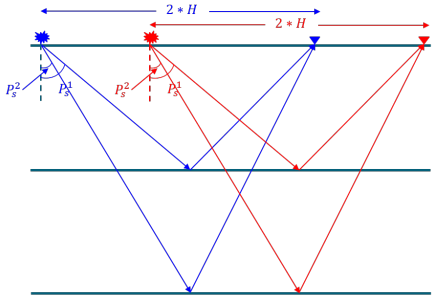

Figure 1: Schematic diagram to show that only two plane-waves are needed for extracting a SOG at $2 \cdot H$ in this simple case.

Moveout analysis of plane-wave in SOGs

Suppose the blue line denotes the physical ray path when the velocity is correct, α is the source take-off angle, d is the true depth, c is the true velocity and h is the half offset from the receiver to the source. The traveltime of the blue line is:

$$t_c = \frac{2d}{c \cdot cos\alpha} \qquad (5)$$

The red line denotes another possible ray path with different take-off angle θ and velocity v, z is the trial depth and H is the half offset from the receiver to the source for the red trajectory. The traveltime of the red line is:

$$t_v = \frac{2z}{v \cdot cos\theta} \qquad (6)$$

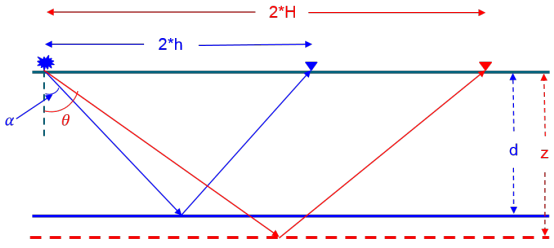

Figure 2: Moveout analysis of plane-wave SOG.

As the blue source and the red receiver are not a real pair, they have an added time shift because of plane-wave encoding. This time shift is:

$$\Delta t = \frac{2(H-h) \cdot sin\theta}{v} \qquad (7)$$

The imaging condition means,

$$t_c = t_v - \Delta t \qquad (8)$$

After derivation using the triangle relationship, we get the depth formula,

$$z = \frac{d(\rho - sin\alpha \cdot sin\theta)}{cos\alpha \cdot cos\theta} \qquad (9)$$

where $\rho = \frac{v}{c}$. To find the stationary point of the depth formula, set $\frac{\partial z}{\partial \theta} = 0$, then we get,

$$\theta = arcsin(\frac{sin\alpha}{\rho}) \qquad (10)$$

At that point,

$$z = \frac{d\sqrt{\rho^2 - sin^2\alpha}}{cos\alpha} \qquad (11)$$

When the velocity is correct, $\theta = \alpha$, $z = d$, which means the final SOGs are mainly derived from the plane-wave with the correct take-off angle; other plane-waves will be stacked destructively.

For the common offset gather, we have

$$\frac{\sqrt{d^2+h^2}}{c} = \frac{\sqrt{z^2+h^2}}{v} \qquad (12)$$

which gives,

$$z = \rho\sqrt{d^2 + \frac{\rho^2-1}{\rho^2}h^2} \qquad (13)$$

using the relationship,

$$h = d \cdot tan\alpha \qquad (14)$$

gives,

$$z = \frac{d\sqrt{\rho^2 - sin^2\alpha}}{cos\alpha} \qquad (15)$$

which is the same as Equation 11. It demonstrates that the plane-wave method generates the correct RMO for SOGs even if the velocity is incorrect.

A simple three-layer model is used to verify the previous derivations. Figure 3 shows the plane-wave gathers for half-offset $h = \pm 600m$ using a correct and wrong velocity. Red dotted

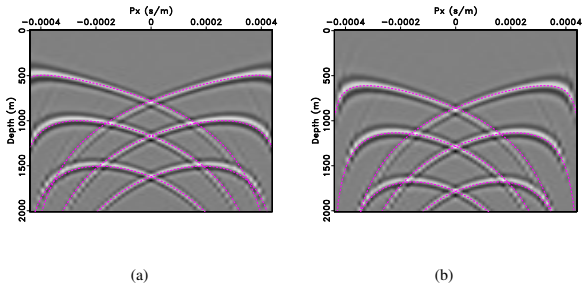

Figure 3: Plane-wave gathers when $h = \pm 600m$ with (a) the correct velocity and (b) the wrong velocity. Red dotted lines show analytical curves given by Equation 11.

lines show the derived $z(p)$ curve (i.e. Equation 11). They are consistent with each other, which means our derivation is correct in the case of constant velocity and a flat layered structure.

Wave-equation tomography with SOGs

For the 2D case, set $\mathbf{x} = (z,x)$ and $\mathbf{h} = h$ in Equation 4. After generating SOGs $I(z,x,h)$, we can extract the RMO information by auto-picking or semi-auto-picking, then back-propagate it to update the velocity model. To find the relationship between RMO Δz and velocity v, we first define the auxiliary objective function:

$$J(\zeta) = \sum_{z_w} I(z+z_w,x,h;c)I(z+z_w+\zeta,x,h;v) \tag{16}$$

for each z, x and h, where c is the true velocity, v is the trial velocity, z_w is the window size and Δz is the depth residual maximizing above objective function, that is,

$$\Delta z = argmax_{\zeta} J(\zeta). \tag{17}$$

Δz satisfies the following equation,

$$g(\Delta z) = \frac{\partial J(\zeta)}{\partial \zeta}|_{\zeta=\Delta z} = 0 \tag{18}$$

that is,

$$g(\Delta z) = \sum_{z_w} I(z+z_w,x,h;c)\frac{\partial I(z+z_w+\Delta z,x,h;v)}{\partial z} \tag{19}$$

Then, the WE tomography operator can be obtained using the rule for an implicit function derivative (Luo and Schuster, 1991; Almomin, 2011; Zhang and Biondi, 2013),

$$\frac{\partial \Delta z}{\partial v} = -\frac{\frac{\partial g(\Delta z)}{\partial v}}{\frac{\partial g(\Delta z)}{\partial \Delta z}} \approx -\frac{\sum_{z_w}\frac{\partial I(z+z_w,x,h;c)}{\partial c}|_v \frac{\partial I(z+z_w,x,h;v)}{\partial z}}{\sum_{z_w} I(z+z_w,x,h;v)\frac{\partial^2 I(z+z_w,x,h;v)}{\partial z^2}} \tag{20}$$

where $\frac{\partial I(z+z_w,x,h;c)}{\partial c}$ is the WE tomography operator using the Born approximation, which is well described for both the one-way wave equation (Sava and Vlad, 2008) and the two-way wave equation (Shen et al., 2012). It's straightforward to extend above formulas to other common image gathers, such as plane-wave domain and angle domain common image gathers.

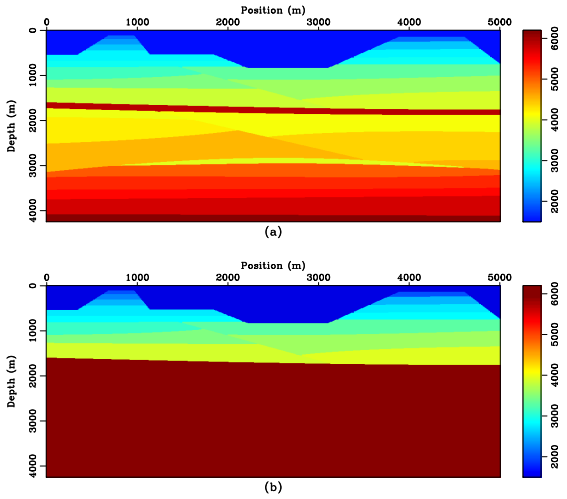

Figure 4: Synthetic case showing (a) true velocity model and (b) initial velocity model.

NUMERICAL TEST

In this section, a synthetic model is used to test WE tomography with SOGs by plane-wave encoding. We also compare the method with WE tomography using plane-wave domain common image gathers (PIGs). Figures 4 (a) and (b) show the true and initial velocity model. The true velocity model has a rugged sea bottom and a thin salt layer, which makes subsalt illumination poor and uneven. In order to demonstrate the advantage of SOGs in building subsalt velocity model, we design an initial model, which has correct velocities above the salt and a constant velocity under the salt. The constant velocity equals to the salt velocity.

To compare SOGs with PIGs fairly, we use the same plane-wave range and sampling rate. Besides, during the iterative inversion, we use the same operators and the same related parameters. Figures 5 (a) and (b) show inverted velocity models using SOGs and PIGs, respectively, after 10 iterations. Compared with the true velocity model, WET with SOGs builds better background velocity than PIGs does. The reason is that, under the salt layer, SOGs provide longer and more reliable RMO information, as indicated in the boxes of figure 6. Figures 7 (a) and (b) show SOGs and PIGs using their own inverted velocity models, as shown in figure 5. We can see that both SOGs and PIGs have already been flattened mostly. However, if we compare their stack images with the stack image using the true velocity model, as figure 8 shows, it's easy to find that the depth of subsalt layers in SOGs is much closer to their true depth. Note that the vertical black lines in figure 8 indicate the position of SOGs and PIGs in previous figures of this section.

CONCLUSION AND DISCUSSION

In this abstract, we applied plane-wave encoding to improve the efficiency of SOG extraction and SOG-based WE tomog-

raphy. Moveout analysis and numerical tests demonstrate the equivalence of plane-wave SOGs and standard SOGs. We also derived the formulas of RMO-based WE tomography and applied plane-wave SOG to velocity estimation. Preliminary comparisons between SOG-based WE tomography and PIG-based WE tomography show that SOGs provide more reliable velocity update information in subsalt areas. More work is needed to analyze the effect of geometric artifacts on SOG-based WE tomography due to multi-pathing in complex areas.

ACKNOWLEDGMENTS

The authors would like to thank Saudi Arabia Oil Company (Saudi Aramco) for its support and permission to publish.

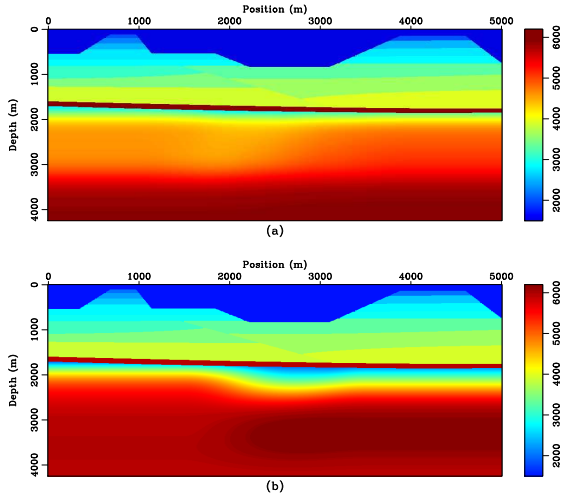

Figure 5: Inverted velocity model of WE tomography using (a) SOGs and (b) PIGs.

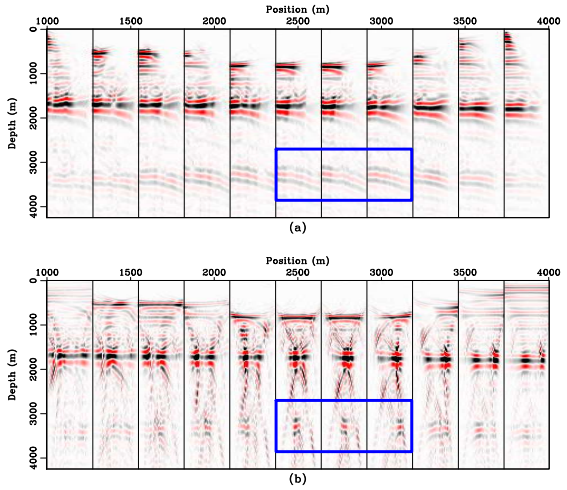

Figure 6: Migrated gathers with the initial velocity model, including (a) SOGs and (b) PIGs.

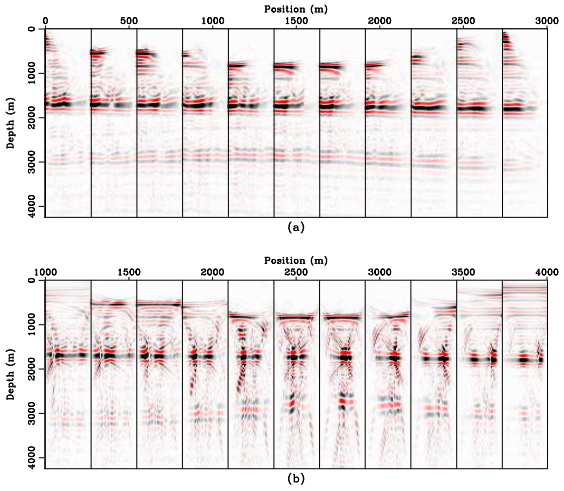

Figure 7: Migrated gathers with the inverted velocity model, including (a) SOGs and (b) PIGs.

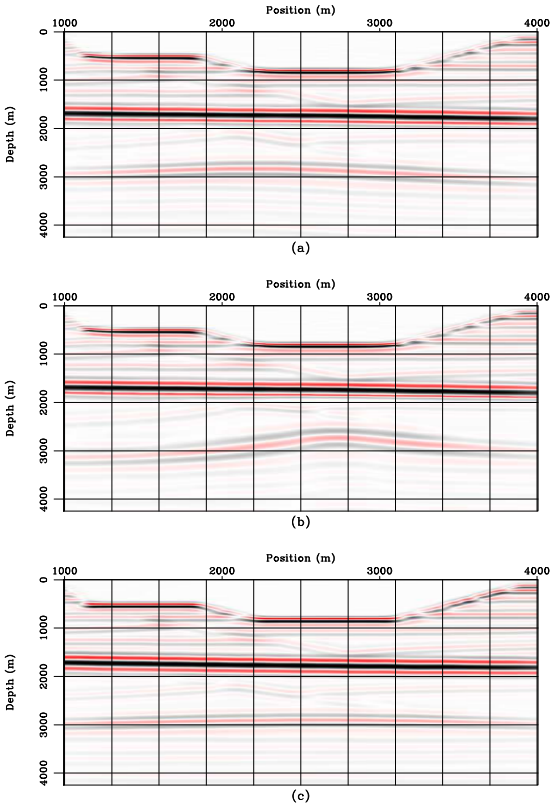

Figure 8: Stack images using (a) the inverted velocity model by SOG-based WE tomography, (b) the inverted velocity model by PIG-based WE tomography and (c) the true velocity model.

EDITED REFERENCES

Note: This reference list is a copyedited version of the reference list submitted by the author. Reference lists for the 2017 SEG Technical Program Expanded Abstracts have been copyedited so that references provided with the online metadata for each paper will achieve a high degree of linking to cited sources that appear on the Web.

REFERENCES

Almomin, A., 2011, Correlation-based wave-equation migration velocity analysis: 81st Annual International Meeting, SEG, Expanded Abstracts, 3887–3891, http://doi.org/10.1190/1.3628017.

Etgen, J., 2012, 3D wave equation kirchhoff migration: 82nd Annual International Meeting, SEG, Expanded Abstracts, 1–5, http://doi.org/10.1190/segam2012–0755.1.

Fleury, C., M. Giboli, and R. Baina, 2014, Moveout analysis for reflection tomography on wave-equation image gathers: 84th Annual International Meeting, SEG, Expanded Abstracts, 4788–4792, http://doi.org/10.1190/segam2014–0052.1.

Giboli, M., R. Baina, L. Nicoletis, and B. Duquet, 2012, Reverse time migration surface offset gathers part 1: A new method to produce classical common image gathers: 82nd Annual International Meeting, SEG, Expanded Abstracts, 1–5, http://doi.org/10.1190/segam2012–1007.1.

Luo, Y., and G. T. Schuster, 1991, Wave-equation traveltime inversion: Geophysics, **56**, 645–653, https://doi.org/10.1190/1.1443081.

Montel, J., 2014, Surface-offset RTM gathers-what happens when the velocity is wrong? 76th Annual International Conference and Exhibition, EAGE, Extended Abstracts, http://doi.org/10.3997/2214-4609.20141484.

Sava, P., and I. Vlad, 2008, Numeric implementation of wave-equation migration velocity analysis operators: Geophysics, **73**, no. 5, VE145–VE159, https://doi.org/10.1190/1.2953337.

Shen, P., 2012, An RTM-based automatic migration velocity analysis in image domain: 82nd Annual International Meeting, SEG, Expanded Abstracts, 1–5, http://doi.org/10.1190/segam2012–0214.1.

Stolk, C. C., and W. W. Symes, 2004, Kinematic artifacts in prestack depth migration: Geophysics, **69**, 562–575, https://doi.org/10.1190/1.1707076.

Stork, C., P. Kitchenside, D. Yingst, U. Albertin, C. Kostov, B. Wilson, D. Watts, J. Kapoor, and G. Brown, 2002, Comparison between angle and offset gathers from wave equation migration and Kirchhoff migration: 72nd Annual International Meeting, SEG, Expanded Abstracts, 1200–1203, http://doi.org/10.1190/1.1816866.

Xu, S., H. Chauris, G. Lambar´e, and M. Noble, 2001, Common-angle migration: A strategy for imaging complex media: Geophysics, **66**, 1877–1894, https://doi.org/10.1190/1.1487131.

Yang, Z., S. Huang, and R. Yan, 2015, Improved subsalt tomography using rtm surface offset gathers: 85th Annual International Meeting, SEG, Expanded Abstracts, 5254–5258, http://doi.org/10.1190/segam2015–5848366.1.

Zhang, W., N. Dai, and Z. Zhou, 2014, Using WEMVA to build salt geometry and sub-salt velocity model: A gulf of mexico test case: 84th Annual International Meeting, SEG, Expanded Abstracts, 992–996, http://doi.org/10.1190/segam2014–0396.1.

Zhang, Y., and B. Biondi, 2013, Moveout-based wave-equation migration velocity analysis: Geophysics, **78**, no. 2, U31–U39, https://doi.org/10.1190/geo2012-0082.1.

Zhang, Y., J. Sun, C. Notfors, S. H. Gray, L. Chernis, and J. Young, 2005, Delayed-shot 3d depth migration: Geophysics, **70**, no. 5, E21–E28, https://doi.org/10.1190/1.2057980.